Spring 5-18-2018

Computational Fluid Dynamics Analysis of Arteriovenous Graft Configurations

Dillon Williams
Washington University in St. Louis

Washington University in St. Louis

School of Engineering and Applied Science

Department of Mechanical Engineering and Material Science

Thesis Examination Committee:
Mohamed Zayed, Chair
Guy Genin
Damena Agonafer

Computational Fluid Dynamics Analysis of Arteriovenous Graft Configurations

by

Dillon Williams

A thesis presented to the School of Engineering and Applied Science
of Washington University in partial fulfillment of the
requirements for the degree of

Master of Science

May 2018
Saint Louis, Missouri

Contents

List of Tables

List of Figures

Acknowledgments

I would like to acknowledge Dr. Mohamed Zayed, Dr. Guy Genin, and Alex Wirtz for their invaluable help

Dillon Williams

Washington University in Saint Louis
May 2018

ABSTRACT OF THE THESIS

Computational Fluid Dynamics Analysis of Arteriovenous Graft Configurations

by

Dillon Williams

Master of Science in Mechanical Engineering

Washington University in St. Louis, May 2018

Research Advisor: Professor Mohamed ZayedProfessor Guy Genin

Hemodialysis is a process of external blood filtration that becomes necessary in the event of end stage renal disease. The most common method of the treatment is the creation of an arteriovenous fistula, which is a surgically created connection between a vein and an artery. For patients who are unable to have an arteriovenous fistula, an arteriovenous graft is required. This graft serves to provide an access site for the removal on unfiltered blood and the return of filtered blood. The design and placement of this graft has not yet been optimized based upon mechanical principles. The aim of this thesis is to evaluate how factors that a surgeon can adjust affect several key parameters that lead to arteriovenous graft failure.

Symbols

m mass

a_n Fourier curve fit parameter

b_n Fourier curve fit parameter

D_h Hydraulic diameter, m

t time, s

u velocity, m/s

ρ fluid density

μ dynamic viscosity

Re Reynolds number

r radius m

α Wormersley number

ω heart rate, 1/s

λ relaxation time

n power index

$\dot{\gamma}$ strain rate 1/s

Abbreviations

AVG Arteriovenous Graft

CFD Computational Fluid Dynamics

Glossary

Anastomosis A connection made surgically between adjacent blood vessels, parts of the intestine, or other channels of the body, or the operation in which this is constructed

Cannulation A technique in which a tube is placed inside a vein to provide venous access

Patency The condition of being open, expanded, or unobstructed

PTFE Polytetrafluoroethylene, a commonly used arteriovenous graft material

Stenosis The abnormal narrowing of a passage in the body

Thrombus A blood clot formed in situ within the vascular system of the body and impeding blood flow.

Preface

In patents undergoing hemodialysis arteriovenous grafts (AVGs) are often a necessary option, however these grafts fail as often as 30% of the time within the first 12 months [23], and as many as 70% of grafts have complications due to stenosis [18] There in a crucial need for improvement of AVG patency and longevity.

Arteriovenous graft failures can largely be attributed to improper blood flow distribution and thrombus formation [12] [10]. Minimizing the occurrence of these factors requires an understanding of the fluid dynamics of blood in the arteriovenous graft system. It is difficult and costly to fully conceptualize blood flow dynamics through in-vivo research. Current technology does not provide a sufficiently robust model of flow dynamics in blood vessels to truly assess complex fluid dynamic problems. The use of Computational Fluid Dynamics (CFD) simulations can greatly elucidate the fluid dynamics of human vasculature and provide insight on the role fluid flow plays in arteriovenous graft failure.

In this study a CFD model has been created using the software package ANSYS Fluent analyze the blood flow in arteriovenous grafts. Various, common graft configuration were constructed and simulated with accurate in-vivo blood flow parameters. Mass flow, wall shear stress, and shear rate were recorded for each AVG configuration to evaluate the impact of graft placement in factors that can lead to arteriovenous graft failure.

Chapter 1

Background

Gradual loss of kidney function eventually leads to End Stage Renal Disease (ESRD). The kidneys are no longer able to filter out excess waste and fluid from the body, which leads to dangerous levels of waste, electrolytes, and fluids in the body [19]. The current standard of treatment of ESRD is hemodialysis, blood is removed from the arterial system and is externally filtered using a dialyzer; the blood is then reintroduced to the venous system. In order to remove blood from the arterial system an access site is created through use of an arteriovenous graft or an arteriovenous fistula. An arteriovenous graft is a bridge between an artery and a vein made of synthetic or biological material, commonly PTFE is the material used for the graft [2]. An arteriovenous fistula is a direct connection between an artery and vein without the use of a bridge. Arteriovenous fistulas are the first choice of treatment because they antogenons and have lower morbidity rates than arteriovenous grafts [2], but sometimes an arteriovenous graft is required. If there is a of lack of suitable vessels or late referral for vascular access and the need for immediate cannulation with avoidance of a central venous catheter, an arteriovenous graft must be used [2].

1.1 Anatomy and Physiology

1.1.1 Overview

Arteriovenous grafts usually connect a. artery to a vein in the arm of the patient. There are two common configurations of the grafts: straight and looped. This study focuses on straight arteriovenous grafts. The placement for a straight graft is shown in figure 1.1

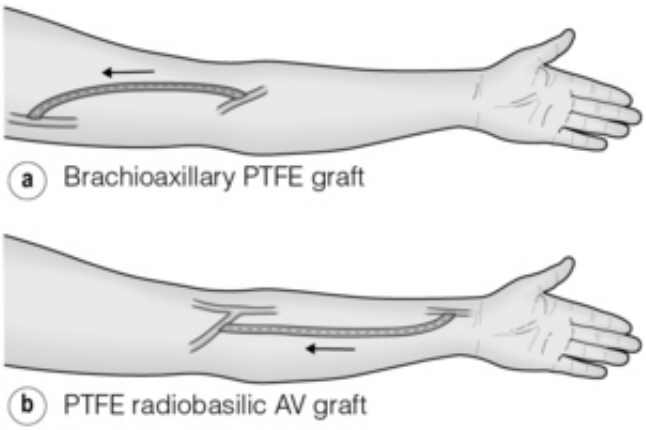

Figure 1.1: Straight configuration of an arteriovenous graft showing two commonly used veins and arteries.

1.1.2 Arteries

The arteries commonly used in arteriovenous grafting are the brachial and radial artery [2]. Brachial arteries range in diameter from 3mm to 5mm [5], and the maximum blood flow velocity ranges from 60 cm/s to 100 cm/s [17] [5]. Radial artery diameters can range from 2mm to 3mm [4], and the blood flow velocity is around 40cm/s during its peak [14].

1.1.3 Veins

The veins commonly considered for arteriovenous grafting are the axillary vein and the basilic vein [2]. The axillary vein diameter ranges from 6mm to 10mm [31] and has a blood flow

velocity of around. The bascilic vein has a diameter ranging between 4mm and 8mm [6] and has a average blood flow velocity of about 20 cm/s [27].

1.2 Arteriovenous Grafts

The general structure of an arteriovenous graft is a tapered tube of roughly 8-10cm with end diameters of 3-4mm and 6-8mm. The smaller diameter end is sutured to the artery in use, the larger diameter end is clipped diagonally to create a hood region and attached to the vein in use. A schematic of the hood region is shown in figure 1.2 [21]

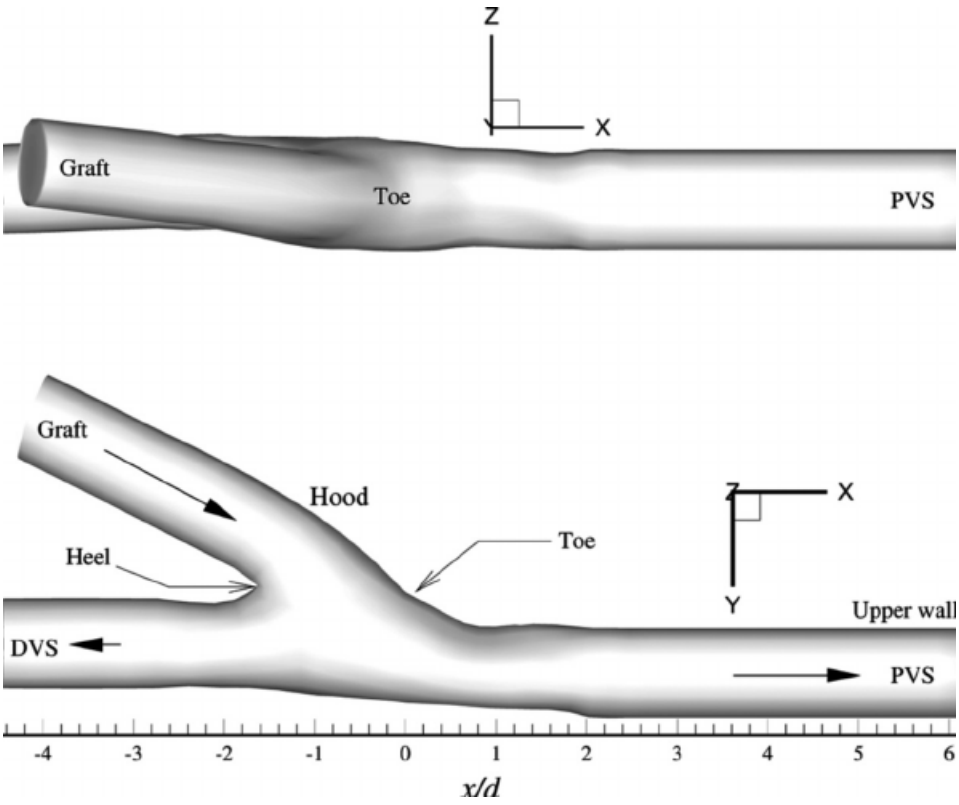

Figure 1.2: Venous anastomosis demonstrating the hooded nature of an arteriovenous graft

1.2.1 Arteriovenous Graft Failure

The main causes for arteriovenous graft failure are inadequate distribution of blood flow [12], thrombosis [10], and high levels of shear stress at the graft vessel connection [30].

If the mass flow is distributed so that the arteriovenous graft does not receive enough blood, the graft will have a high chance of failure within a few months. Conversely, if the graft receives too much blood a phenomenon called steal syndrome is observed. Steal syndrome is when not enough blood goes to the distal artery, thus depriving the lower arm and extremities of vital nutrients which can lead to pain, paresthesia, or gangrene [24]. Studies have shown that less than 40-50% of blood flow to the arteriovenous graft greatly increases the risk of failure [28], and flow to the graft of greater than 70% leads to steal syndrome. [26].

Thrombus formation is one of the main causes of graft failure and complications. Platelet play an integral role in the development of thrombi though platelet adhesion, aggregation, and cohesion [13]. High shear environments lead to greatly increased thrombus formation due specifically to increased platelet adhesion and aggregation. High shear stress on the vessel walls as well and high shear rates within the blood both lead to increased thrombus formation due to platelets [34] [13] [38]. In addition high levels of shear stress at the graft vessel connection can induce and exacerbate intimal hyperplasia [30]. Intimal hyperplasia, which is the thickening of the tunica intima of a blood vessel, eventually leads to stenosis and requires surgical intervention to salvage the blood vessel [32].

Failed arteriovenous grafts lead to increased patient morbidity and associated medical costs. It is the goal of this study to understand if and how these failure risks depend on the placement of an arteriovenous graft in the hope that these risk factors can be reduced with more optimal configuration of the AVG.

1.3 Fundamental Biofluid Dynamics

To gain an initial understanding of the problem it is beneficial to estimate the range of the Reynolds number. Equation 1.1 is the Reynolds number for pipe flow, which is what is being simulated in this study. The Reynolds number will give an idea of if the fluid will

be laminar, transitional, or turbulent. If the Reynolds number is 2000 or less the flow is considered laminar, a Reynolds number between 2000 and 4000 is transitional flow, and a Reynolds number greater the 4000 is turbulent [37]. In equation 1.1 ρ is the fluid density, u is the fluid velocity, D_H is the hydraulic diameter which for circular pipes is just the diameter, and μ is the dynamic viscosity.

$$Re = \frac{\rho u D_H}{\mu} \tag{1.1}$$

The Navier-Stokes in three dimensions was solved using the finite volume method.

$$\frac{\partial}{\partial t}(\rho u_i) + \frac{\partial}{\partial x_j}(\rho u_i u_j + p\delta_{ij} - \tau_{ji}) = 0 \tag{1.2}$$

In this equation τ_{ji} is the stress tensor which is as follows

$$\tau_{ij} = \mu_{eff}(\dot{\gamma}) \left(\frac{\partial u_i}{\partial x_j} + \frac{\partial u_j}{\partial x_i} \right) \tag{1.3}$$

1.3.1 Pulsatile Flow

When analyzing the fluid dynamics of the vascular system it is necessary to take into account the pulsatile nature of blood flow. For an incompressible fluid in a tube, simple pulsatile flow can be represented by:

$$\rho \frac{\partial u}{\partial t} = -\frac{\partial p}{\partial x} + \mu \left(\frac{\partial^2 u}{\partial r^2} + \frac{1}{r} \frac{\partial u}{\partial r} \right) \tag{1.4}$$

where ρ is the fluid density, μ is the viscosity, p is the pressure, and r is the radius from the center of the artery.

Further complexities of pulsatile flow can be modeled; a commonly used parameter to define the velocity profile is the Wormersley number [22]. The Wormersley number is a ratio of the inertial forces to viscous forces that is adjusted for pulsatile flow, which is as follows:

$$\alpha = R\left(\frac{\omega\rho}{\mu}\right)^{1/2} . \tag{1.5}$$

In this equation ω to the heart rate in radians per second, ρ is the fluid density, d is the diameter of the artery, and μ is the fluid viscosity. If $\alpha < 2$, viscous forces dominate the flow; the pulse is considered quasi-static and the velocity profile is relatively parabolic. If $\alpha > 2$, the inertial forces are dominant and the velocity profile is more complex. In peripheral veins and arteries the Wormersley number is between 2 and 3.

1.3.2 Non-Newtonian Nature of Blood

Blood behaves as a non-Newtonian pseudo-plastic, and is best modeled in oscillatory flow by the Bird-Carreau model [16] [33]. The Bird-Carreau model represents the viscosity μ_{eff} as a nonlinear function of shear rate. The dependence is as follows

$$\mu_{eff}(\dot{\gamma}) = \mu_{\text{inf}} + (\mu_0 - \mu_{\text{inf}})\left(1 + (\lambda\dot{\gamma})^2\right)^{\frac{n-1}{2}} \tag{1.6}$$

$\dot{\gamma}$ is the shear rate

$$\dot{\gamma}_{ij} = \frac{\partial u_i}{\partial x_j} + \frac{\partial u_j}{\partial x_i} \tag{1.7}$$

Chapter 2

Geometry and Mesh Generation

2.1 Geometry

The geometry was created using ANSYS DesignModeler; the specific layout was created to best model the placement of a straight arteriovenous graft connecting an artery to a vein. Figure 2.1 shows the geometry and depicts the artery inlet and outlet, the vein inlet and outlet. To analyze the spectrum of possible configurations the diameter of the artery was simulated at 3mm, 4mm, and 5mm. The diameter of the vein was simulated at 6mm, 8mm, and 10mm. Each arterial diameter was analyzed with each venous diameter for a total of nine different combinations.

The dimensions for the geometry were motivated by estimations of physiological dimensions of arteries and veins. The diameters of the brachial and radial arteries both fit within the range of 3mm to 5mm, and the diameters of the axillary and basilic veins both fit in the range of 6mm to 10mm. The length of the AVG was 150mm pm 2mm depending on the angle of attachment at the artery. The diameter of the arterial attachment of the AVG was 4mm for the 4mm and 5mm diameter artery geometries, and 3mm for the 3mm diameter artery geometries. The venous attachment of the arteriovenous graft was slanted to create a toe region, as shown in figure 2.2. The graft attachment to the vein created an elleptical plane of attachment with a semiminor axis length of 7mm and a semimajor axis length of 8.5mm. In the case of the 6mm diameter vein the semiminor axis was 6mm and the semimajor axis was 7.5mm.

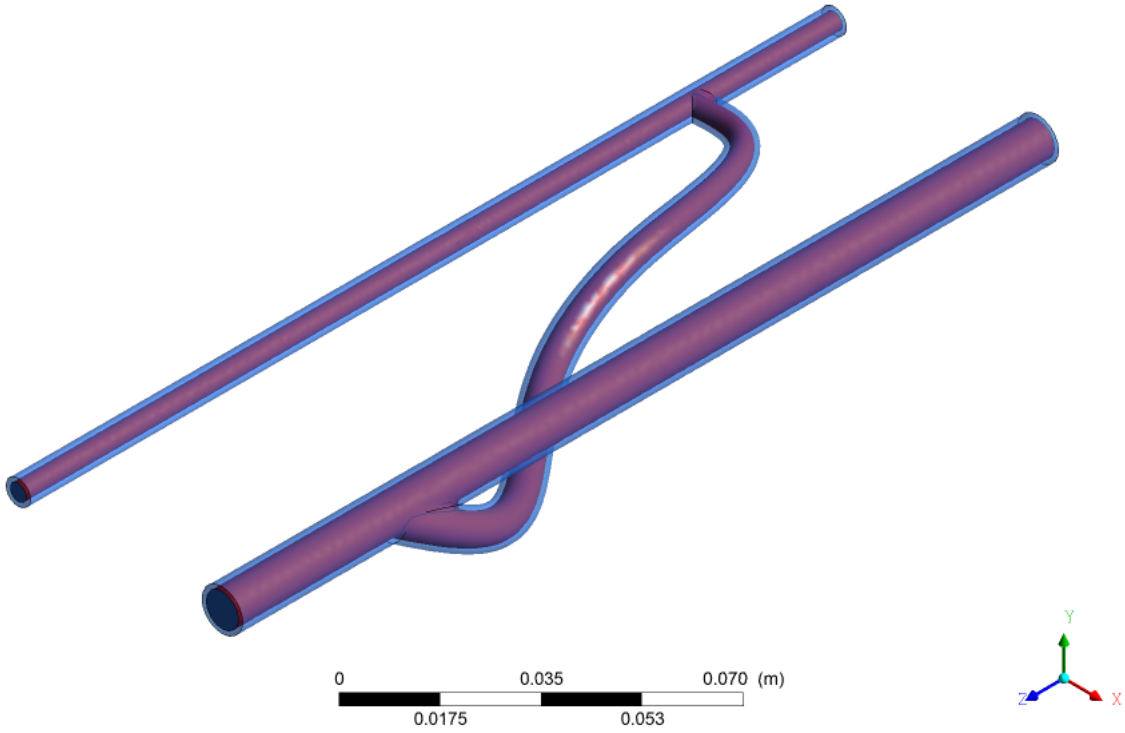

Figure 2.1: Geometry of the artery, vein, and arteriovenous graft: 4mm diameter artery, 8mm diameter vein, 90 degree angle of attachment

The angle of attachment of the arteriovenous graft to the artery was varied to examine the effects of arterial attachment. The angle of attachment, shown in figure 2.3, is measured from the direction of blood flow in the artery. The angles simulated were 30, 60, 90, 120, and 150 degrees from the direction of flow.

2.2 Mesh

Meshing for this geometry was done in the ANSYS Fluent Meshing software. Due to the large amount of curvature in the model, the size function chosen for meshing was the curvature. The curvature size function in the Fluent Meshing software examines the curvature on the edges and faces of the geometry and ensure that the meshing does not violate the maximum allowed element size or the curvature normal angle. In the curvature size function there are

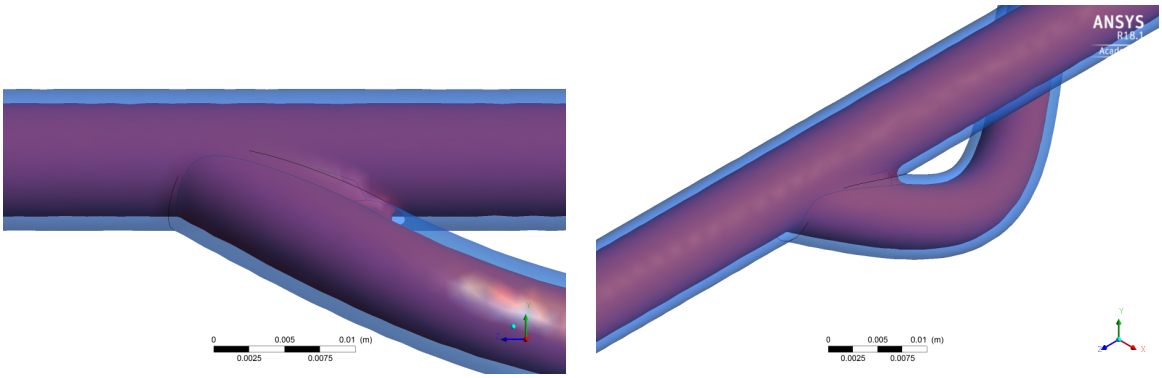

Figure 2.2: Graft attachment to the vein with a hood region

three controls to further refine the mesh: the relevance center, the span angle center and the transition. Relevance center sets the relevance of the meshing which defines how fine the mesh will be. In this simulation the relevance was set to an intermediate value that was optimized for convergence. The span angle center, which sets the goal for the amount of elements on a curved surface, was also in this optimized range. The transition mesh control affects the rate at which adjacent mesh elements will grow, and was set to provide a smooth transition. [3]

The goal of this meshing regime was foremost to create an adequately fine mesh to resolve the physics of the model in a way that reached numerical convergence, but not a mesh that was unnecessarily complex and would drastically slow computational time. The secondary goal of this meshing scheme was to define a reproducible mesh as to standardize the number of elements and mesh quality for all forty-five different AVG configurations.

The number of elements for each simulation ranged between 110,000 and 150,000 elements. All the elements were tetrahedral. A sample mesh for a 4mm artery diameter, 8mm vein diameter, and 90 degree graft attachment is shown in figure 2.4 and figure 2.5

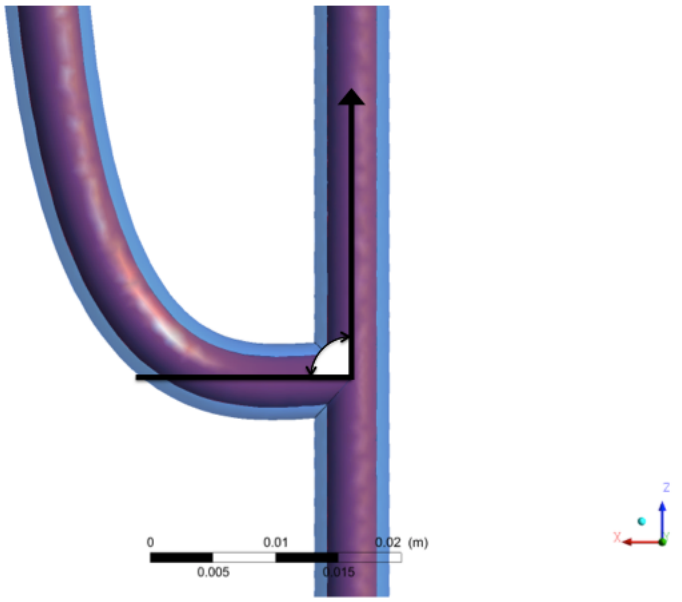

Figure 2.3: Angle of attachment to the artery, measured from the direction of blood flow

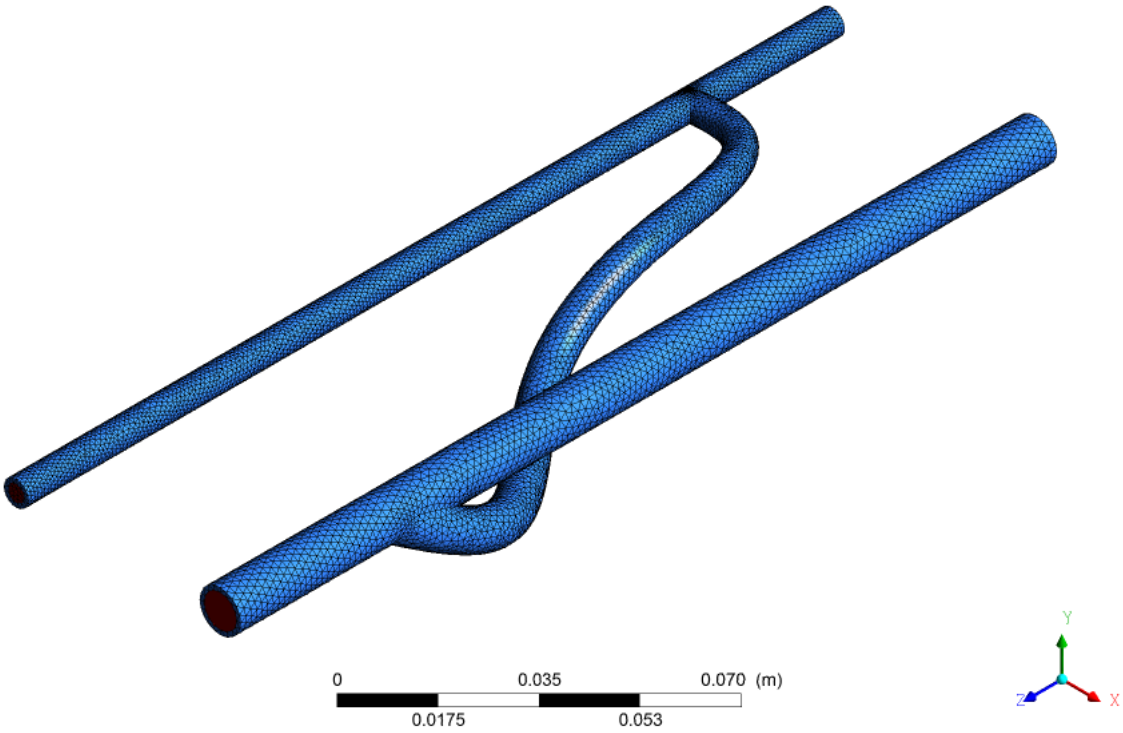

Figure 2.4: The meshing solid section of the geometry.

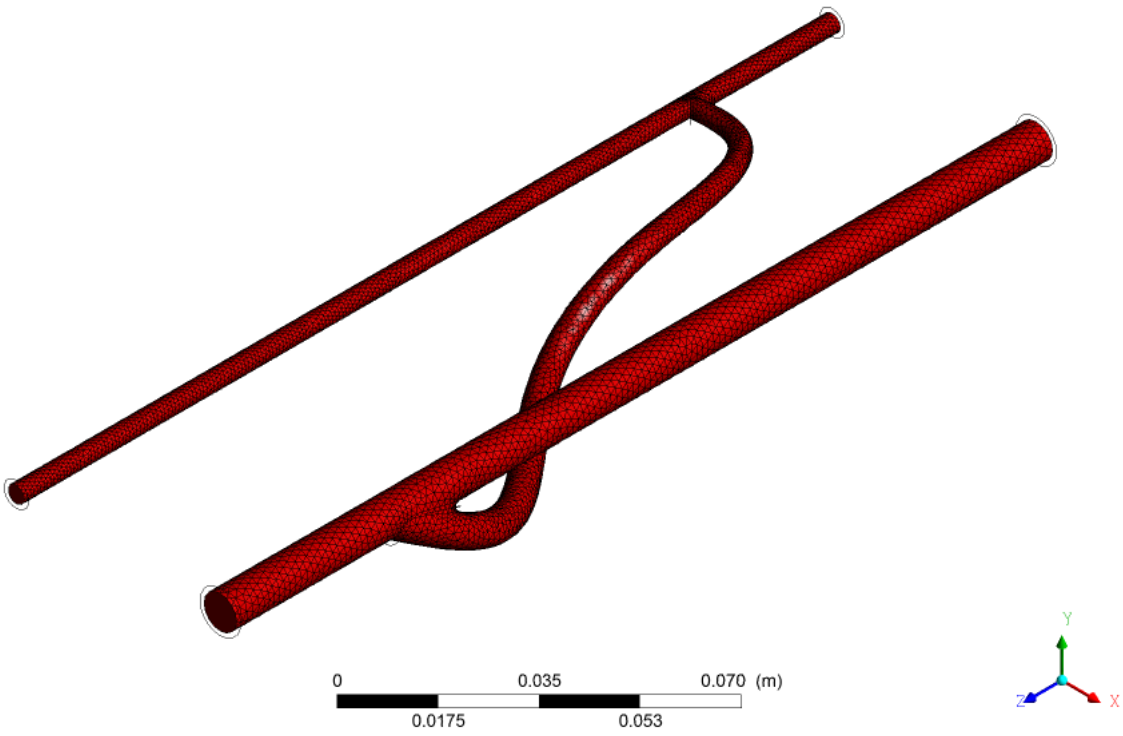

Figure 2.5: The meshing of the fluid section of the geometry.

Chapter 3

Methods

3.1 Physical Setup

This study utilized a CFD pressure based, transient simulation to accurately model the pulsatile flow of blood in an arteriovenous system with a graft in place.

3.1.1 Model

This simulation utilized a viscous laminar model. Preliminary estimations of the Reynolds number in the simulation 1.1 predicted a maximum value of 1330 which is within the laminar range. This estimation was calculated using a maximum velocity of .8m/s, arterial diameter of 5mm, blood density of 1060 kg/m^3, and blood dynamic viscosity of $.0035 Pa * s$. This was just a preliminary estimate, but it gave good reason to use the viscous laminar model.

3.1.2 Material Properties

The material model for blood was the Bird-Carreau model (equation 1.6). The density and values used in the Bird-Carreau are presented in table 3.1

Table 3.1: Material Properties of Blood [25]

Density (kg/m^3)	1060
Viscosity at zero shear rate μ_0 ($Pa * s$)	.0056
Viscosity at infinite shear rate μ_{inf} ($Pa * s$)	.0035
Relaxation time λ (s)	3.313
Power Index n	0.3568

3.1.3 Boundary Conditions

Boundary conditions were created at the arterial inlet and outlet and the vascular inlet and outlet as shown in figure 3.1.

The fluent user guide recommends using velocity functions as inlet conditions for incompressible flow[3].

Inlet Boundary Conditions

The inlet condition for the artery was modeled from velocity wave forms measured in the radial and brachial arteries [5] [14]. Gaussian wave fitting was used to best recreate the wave form, this process is in utilized other studies attempting to fit arterial velocity wave forms [9]. The Gaussian fit wave form was converted to a Fourier series as this was found to work better with the ANSYS Fluent user defined functions environment.

$$f(t) = a_0 + \sum_{n=1}^{\infty} a_n \cos(\omega n t) + \sum_{n=1}^{\infty} b_n \sin(\omega n t) \tag{3.1}$$

Equation 3.1 shows the function for a Fourier Series where a_n and b_n are the curve fit parameters, t is the simulation time. ω is the function frequency, adjusting this allows effective control of simulated heart rate. The Fourier series fitting was done in MATLAB (Mathworks, Inc) and created eight terms. The coefficients and frequency can be found in Appendix A. Figure 3.2 shows the resulting function that was used as the arterial inlet velocity.

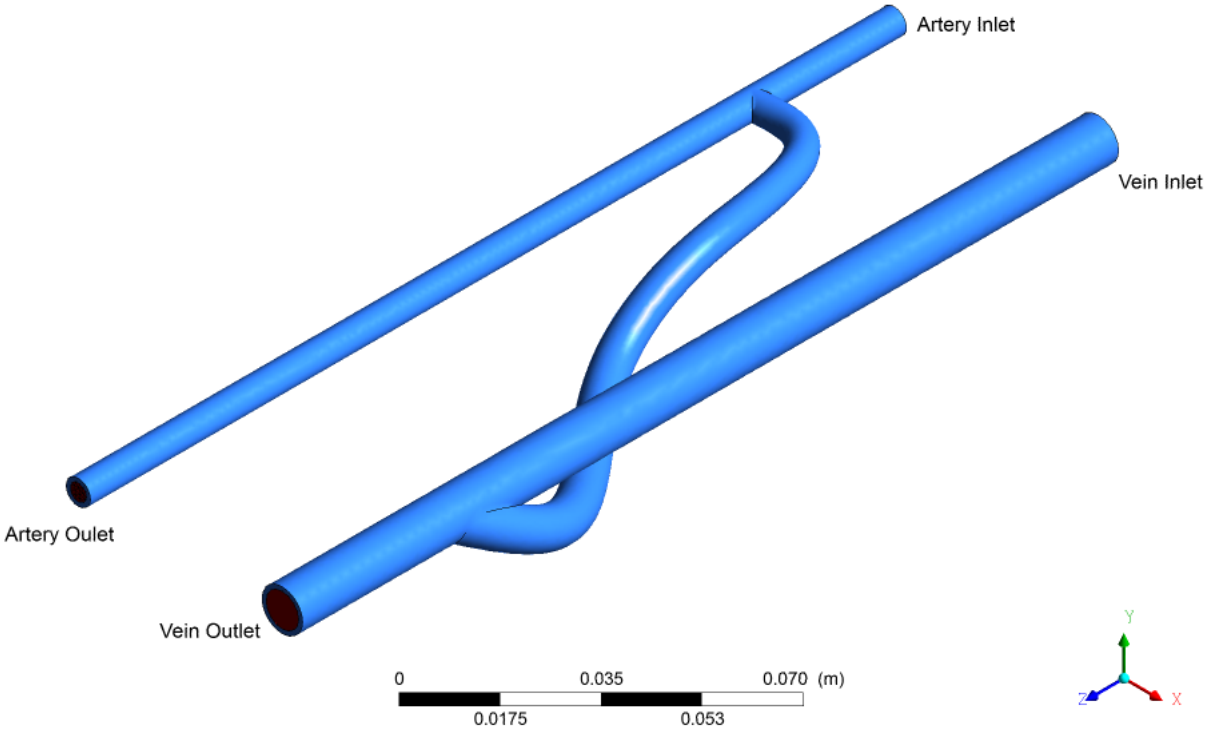

Figure 3.1: Schematic of the inlet and outlets of the artery and vein

The venous system does not experience significant pulsatile flow [11]. For the vein inlet condition a constant velocity of 15cm/s was used. This is representative of the flow in the axillary and basilic veins [27]

Outlet Boundary Conditions

Outlet boundary conditions create an interesting problem for vascular flow. The Fluent User Guide recommends using pressure outlet conditions for pipe flow [3], but this fails to account for the downstream effects that are present in the circulatory system. Many studies utilize the outflow boundary condition when simulating vascular systems [36] [35]

The inflow was distributed so that 90% was sent to the graft and 10% of the flow was sent to the distal artery. This is in accordance with National Kidney Foundation KDOQI Clinical Practices [29].

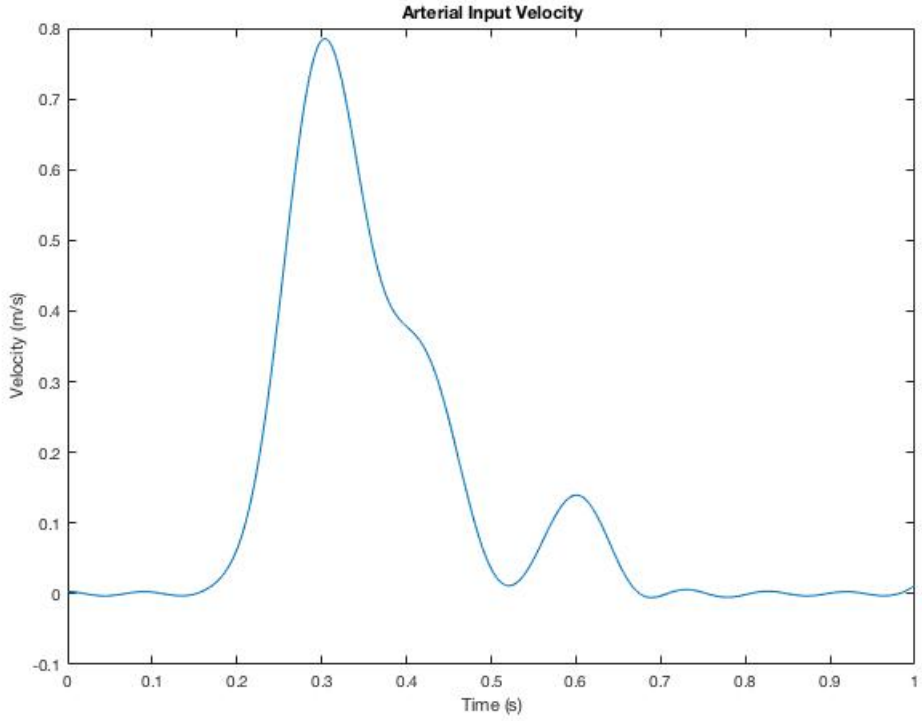

Figure 3.2: Function of the arterial inlet velocity

In the vein the outflow boundary condition further distributed the flow from the graft so that 85% of the inflow went to the proximal vein and 15% of the inflow went to the distal vein.

3.2 Solution Setup

3.2.1 Solution Methods

The solver chosen for this simulation was the ANSYS Fluent CFD solver. ANSYS Fluent is a powerful and accurate tool for solving fluid dynamic simulations, especially for internal flow systems with low Reynolds number. The SIMPLE pressure-velocity coupling method was used with second order spatial discretization and first order transient discretization. The PISO pressure-velocity coupling method with second order spatial discretization and

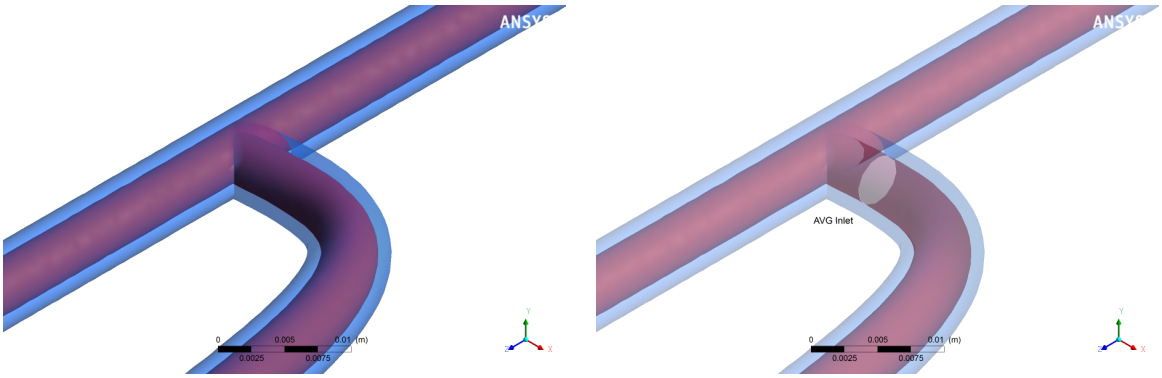

Figure 3.3: Zone plane created at the AVG inlet

transient discretization was used without noticeable difference in results but increased computation time. The fluid dynamics of the simulation were not incredibly complex and the time step was small, so the SIMPLE pressure-velocity coupling method with second order spatial discretization and first order transient discretization was sufficient.

3.2.2 Reports

Output reports were created to analyze arterial mass flow, AVG mass flow, wall shear stress, and shear rate. The arterial mass flow was measured at the arterial inlet, and the AVG mass flow was measured at a user defined plane created at the attachment of the AVG to the arterial wall. This plane can be seen in figure 3.3

The wall shear stress was measured at every time step for each cell of the system in the solid domain; this included the artery, vein, and arteriovenous graft. The shear rate was measured at every time step for each cell of the system in the fluid domain, which was the blood.

3.2.3 Initialization and Calculation

Initialization of the simulation was done through hybrid initialization. The Fluent hybrid initialization functions by solving Laplace's equation (equation 3.2) with appropriate boundary conditions to estimate a velocity field [3]

$$\nabla^2 \varphi = 0 \tag{3.2}$$

In Laplace's equation φ is the potential which is defined in equation 3.3

$$\vec{V} = \nabla \varphi \tag{3.3}$$

Boundary conditions used in hybrid initialization are those of the walls, inlets, and outlets of the system. The constraints for these boundary conditions during hybrid initialization are shown in equations 3.4

$$\left.\frac{\partial \varphi}{\partial n}\right|_{Wall} = 0 \tag{3.4}$$

$$\left.\frac{\partial \varphi}{\partial n}\right|_{Inlet} = V_{\perp} \tag{3.5}$$

$$\varphi_{OutIet} = 0 \tag{3.6}$$

For the transient calculation a time step of .01 s was utilized with 100 time steps. The configuration was chosen in order to simulate one pulse with high accuracy. The maximum iterations per time step allowed was set to 200 as this was found to be sufficient to reach the convergence criteria on each time step. The convergence criteria for the continuity, x-velocity, y-velocity, and z-velocity were all set at an absolute tolerance of .001. The scaled residuals of the transient simulation are shown in figure 3.4.

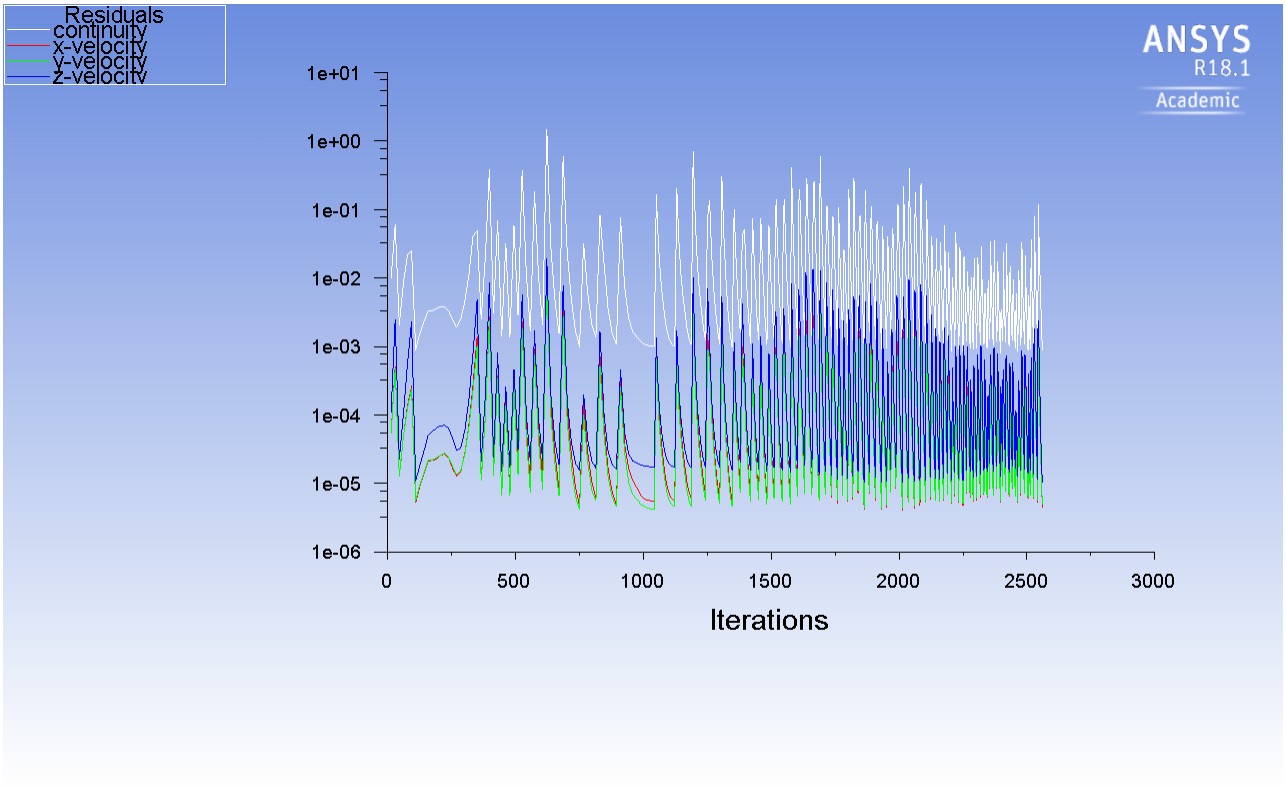

Figure 3.4: The scaled residuals of the transient simulation

Chapter 4

Results

4.1 Mesh Independence Study

A mesh independence study was performed to ensure a fine enough mesh was utilized so that the solution converged to one that was independent of mesh size. The mass imbalance of the transient simulation was measured with mesh the amount of mesh elements ranging from 13,000 elements to 260,000 elements. The amount of elements was capped at 512,000 as this study used an academic license of ANSYS Fluent. The mesh independence study showed that beyond about 100,000 elements the solution was independent of mesh size, as shown in figure 4.1.

4.2 Transient Results

The main goal of this CFD study was to assess the dependence of factors that lead to AVG failure on the placement of the AVG. The mass flow ratio was measured and these values of these variables are presented in a heat map format to best compare the fort$y$-five different simulations. The y-axis of the heat maps is the angle of attachment increasing from 30 degrees to 150 degrees. The x-axis is the diameter of the artery and the diameter of the vein; the labeling is structured with the first numerical value as the arterial diameter and the second numerical value as the venous diameter. The x-axis is organized in order of increasing ratio of artery diameter to vin diameter. The AVG configuration to 3mm artery diameter and 10mm vein diameter is in the first bin on the x-axis as this is the largest discrepancy between

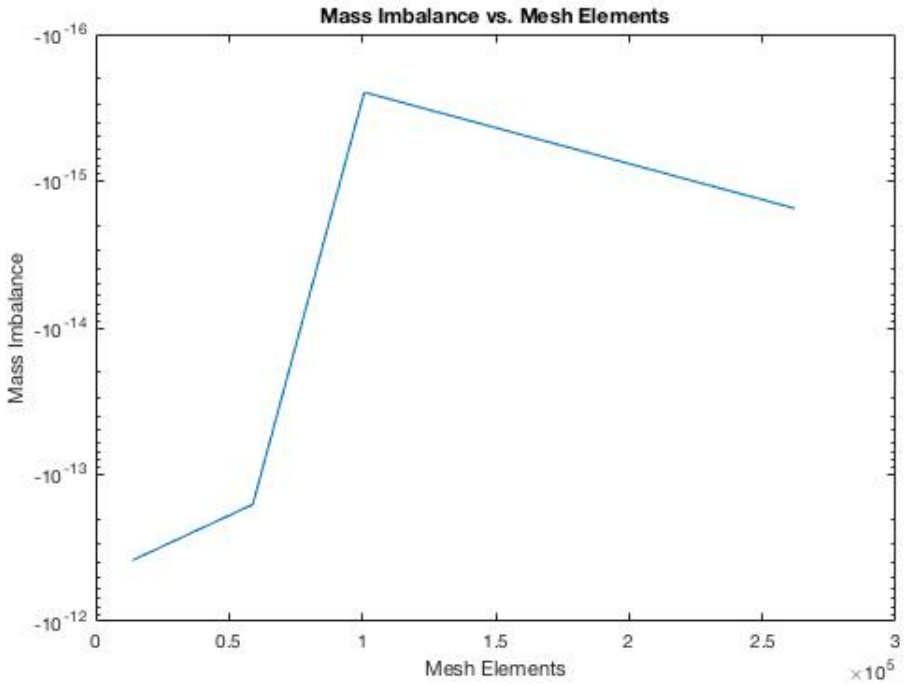

Figure 4.1: Mass imbalance as a function of mesh elements in the simulation

diameters, and the AVG configuration of 5mm artery diameter and 6mm vein diameter is in the last bin on the x-axis as this is the smallest discrepancy between diameters. Once the mass flow ratio data was analyzed, a suitable range was determined using reference values from the National Kidney Foundation [29]. Within this range the wall shear stress and blood shear rate were anaylzed.

4.2.1 Mass Flow

The transient simulation recorded the mass flow into the arterial inlet as well as the mass flow into the arteriovenous graft at the location it is attached to the artery. For each configuration the arterial mass flow was compared to the arteriovenous graft mass flow. An an example of the mass flow for the artery and the AVG can be seen in figure 4.2. The total mass flow across these boundaries was summed and presented as a fraction. Figure 4.3 is a heat map of the mass flow ratio for each of the forty five AVG configurations. From this data the following artery vein diameter pairs give a mass flow ration within the range of 40% to

70%; 3mm to 6mm, 4mm to 8mm, 5mm to 10mm, 5mm to 8mm, and 4mm to 6mm. These configurations were used to further study the wall shear stress and blood shear rate.

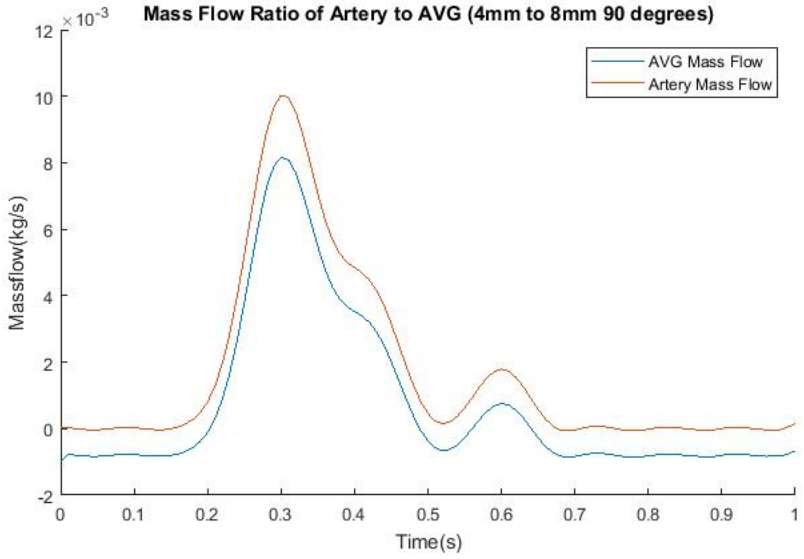

Figure 4.2: A sample plot of mass flow through the arterial inlet and AVG inlet as a function of time

4.2.2 Wall Shear Stress

Wall shear stresses cause a multitude of problems in AVGs, most notably platelet activation which leads to the development of thrombi [13]. In his work James Hathcock has shown that platelet activation and adhesion occurs at around 10 Pa. To best analyze the shear stress in the system this study recorded amount of surface area that was above the threshold level of 10 Pa. A transient study was performed to show the precent of surface area above the threshold shear stress during the blood pulse. Figure 4.4 shows this data in the form of five plots; one for each diameter pair. Within each plot the percent of surface area above the threshold for each angle of attachment is shown.

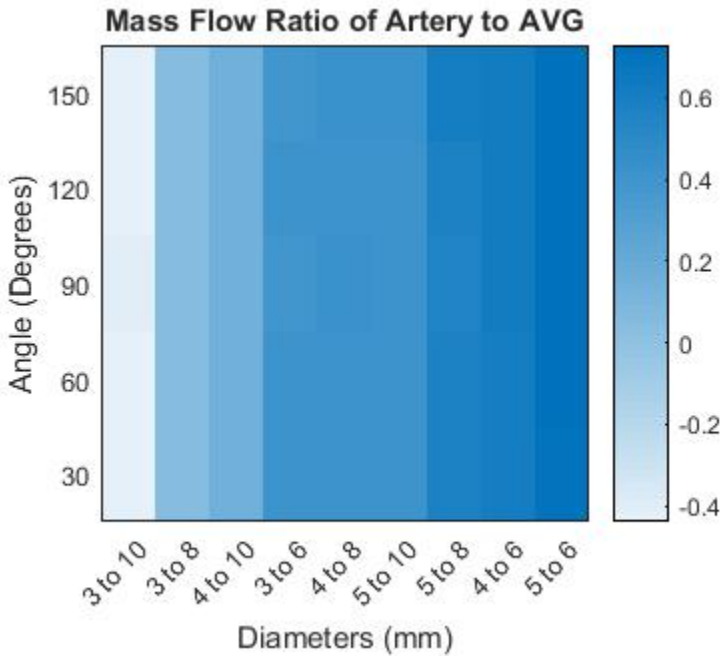

Figure 4.3: A heat map of the mass flow ratio in each AVG configuration

4.2.3 Shear Rate

High levels of shear rate within the blood has been shown to increase the instances of platelet micro thrombi formation. Around 1000-2000 1/s of shear rate this development of micro thrombi becomes significant [34]. For the analysis of blood shear rate this study took a similar approach as the wall shear stress. A threshold rate of 2000 1/s was chosen and the percent of blood that surpassed this threshold was measured for each configuration. These results can be seen in 4.5

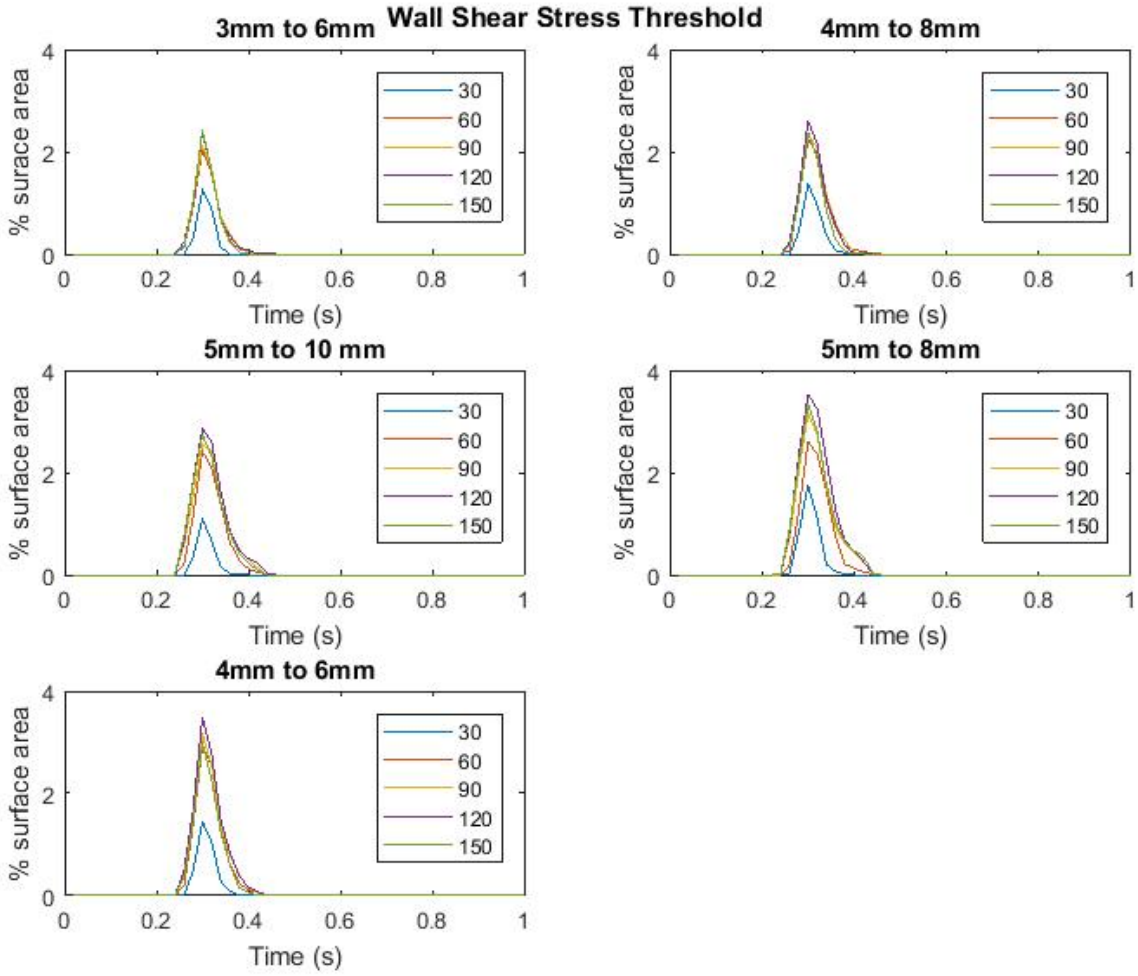

Figure 4.4: Percent of the wall surface area above 10 Pa of shear stress for each diameter pair and each angle of attachment

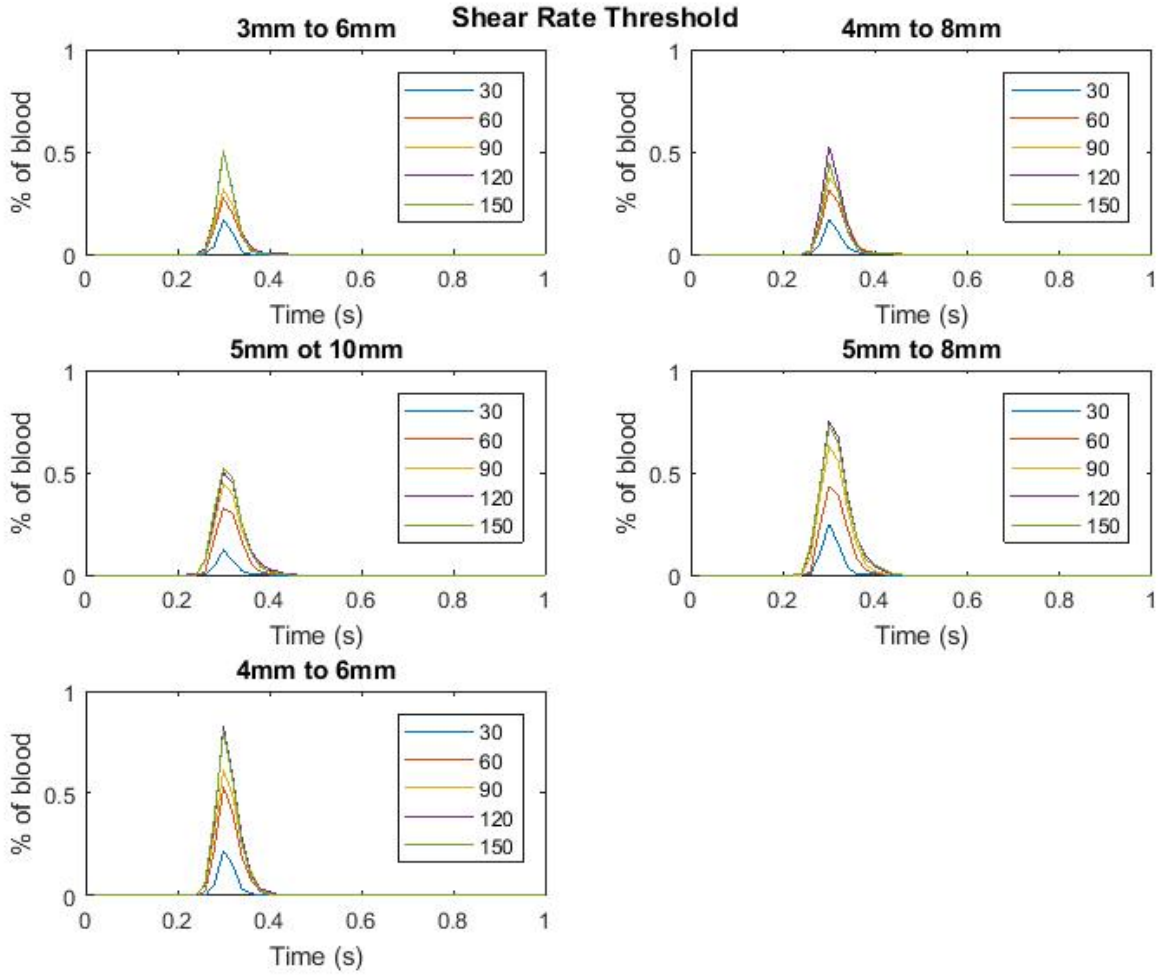

Figure 4.5: Percent of the blood above 2000 1/s of shear rate for each diameter pair and each angle of attachment

Chapter 5

Discussion

5.1 Mass Flow

The mass distribution in the arteriovenous graft system showed a clear dependence on blood vessel diameter ratio, and virtually no dependence on angle of attachment to the artery. As mentioned in the background section of this study, improper mass distribution can lead to graft failure and steal syndrome. Both complications are incredibly detrimental to the patient. Based on current literature on the topic the suggested mass distribution ranges from 40% to 70% of blood flow directed from the artery to the arteriovenous graft. To stay within the optimal blood flow distribution the data in this study suggests a ratio of arterial diameter to vein diameter between 1:2 and 2:3. The heat map in figure 4.3 shows this optimal range being achieved by geometries with the following arterial diameter to vein diameters; 3 mm to 6 mm, 4 mm to 8 mm, 5 mm to 10 mm, 5 mm to 8 mm, and 4 mm to 6 mm.

5.2 Wall Shear Stress

The wall shear stress showed an interesting dependance on angle of attachment to the artery. By far the the lowest amount of surface area above 10 Pa was recorded at a 30° angle of attachment, and the highest amount of surface area above 10 Pa of shear stress were recorded at a 120° angle of attachment. However for all diameter pairs except 5mm to 8mm 60°, 90°, 120°, and 150° angle of attachment all showed a similar amount of surface area above the 10 Pa threshold.

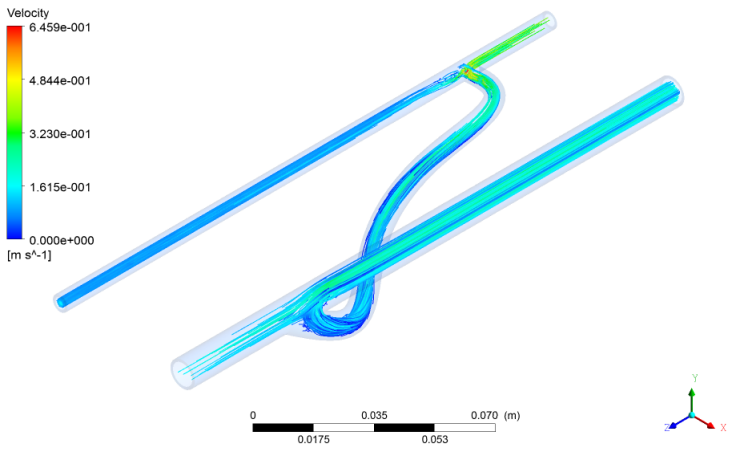

Figure 5.1: A schematic of the stream lines in the AVG configuration with a 4mm diameter artery, 8mm diameter vein, and 90° angle of attachment

5.3 Shear Rate

Shear rate within the blood has a a clear dependence on the angle of attachment to the artery. A 30° anastomosis led the the lowest percent of blood below a shear rate of 2000 1/s. The amount of blood above this threshold increased with increasing angle up to 120°. 150° angle of attachment showed either a slightly lower amount of blood above the threshold or the same amount of blood as the 120° angle of attachment.

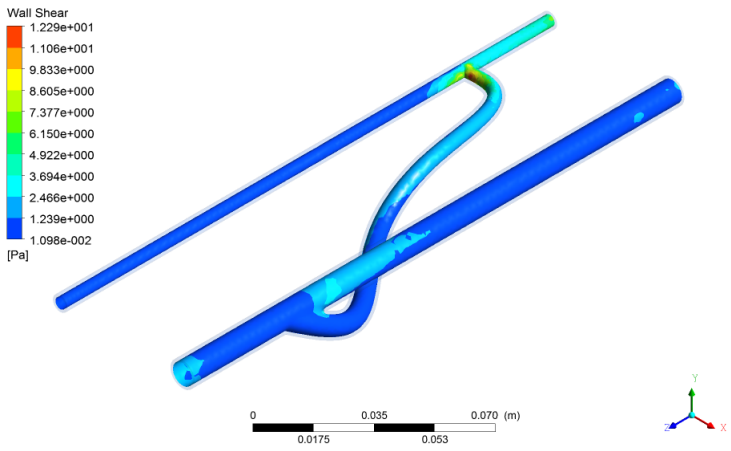

Figure 5.2: A schematic of the wall shear stress in the AVG configuration with a 4mm diameter artery, 8mm diameter vein, and 90° angle of attachment

5.4 Recommendations

This study examined a simple model problem to explore how an arteriovenous graft could be optimized. The model problem showed several clear trends that lend insight into improved arteriovenous graft design.

Based upon the results of the study, the optimal configuration of an arteriovenous graft should have a ratio of arterial diameter to venous diameter between 1:2 and 2:3 with a preference towards arterial diameter 4mm or larger and a venous diameter larger than 6mm. In addition the angle of attachment should be between 30°s and 90°s. This configuration will result in a mass flow distribution between 40% and 70% while minimizing shear stresses and shear rate.

5.5 Future Work

An important physical aspect of vasculature that was not in the scope of this study is the deformability of vessel walls. Arterial walls are not rigid and vein walls are in fact relatively flexible. The next step of this study would be to model the artery and vein as deformable

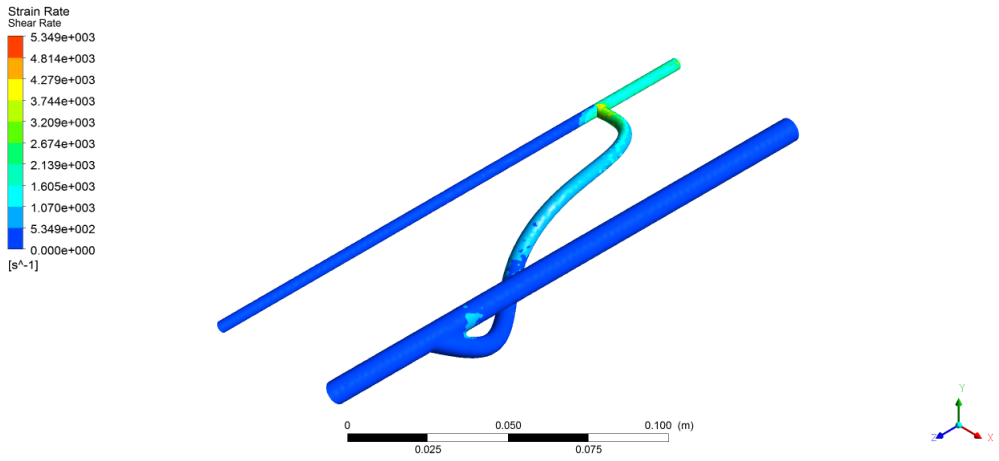

Figure 5.3: A schematic of the blood shear rate in the AVG configuration with a 4mm diameter artery, 8mm diameter vein, and 90° angle of attachment

bodies with proper biosolid properties and then utilize a fluid-structure integration package to simulate the blood flow through non-rigid vessels.

Beyond the fluid simulation aspect of arteriovenous graft integrity it is incredibly important to consider the materials science aspect of the problem. Research regarding the usage of biomaterials for arteriovenous grafts shows strong evidence that well-chosen biomaterials can lead to significantly higher patency rates in arteriovenous grafts compared to the current synthetic materials being used [8]. This factor, when combined with the structural optimization in this thesis, may lead to further improvements in patient outcomes.

Appendix A

Fourier Series

This section defines the Fourier series used to create the arterial inlet velocity function

$f(t) = a_0 + a_1 cos(tw) + b_1 sin(tw) + ... + a_8 cos(8tw) + b_8 sin(8tw)$

Table A.1: Fourier series coefficients for the arterial inlet velocity function

Coefficients	**value (with 95% confidence bounds)**
a_0	0.1626 (0.1607, 0.1645)
a_1	-0.2171 (-0.2219, -0.2122)
b_1	0.1255 (0.12, 0.131)
a_2	0.0225 (0.01458, 0.03042)
b_2	-0.1591 (-0.1604, -0.1577)
a_3	0.06232 (0.05433, 0.07031)
b_3	0.08745 (0.0831, 0.09179)
a_4	-0.02844 (-0.02983, -0.02704)
b_4	0.0121 (0.01074, 0.01346)
a_5	-0.01337 (-0.02117, -0.005573)
b_5	-0.05399 (-0.05741, -0.05057)
a_6	0.01706 (0.00971, 0.0244)
b_6	0.03315 (0.03125, 0.03505)
a_7	-0.0101 (-0.01169, -0.008523)
b_7	-0.002116 (-0.003801, -0.0004319)
a_8	0.007929 (0.006185, 0.009673)
b_8	-0.00475 (-0.007728, -0.001773)
w	7.577 (7.494, 7.66)

References

[1] Marine hydrodynamics, Fall 2004.

[2] Jacob A Akoh. Prosthetic arteriovenous grafts for hemodialysis. *J Vasc Access*, 10(3):137–147, 2009.

[3] ANSYS. *ANSYS FLUENT 12.0 User's Guide*.

[4] Tariq Ashraf, Ziauddin Panhwar, Sultana habib Habib, Muhammad Anis Memon, Fahad Shamsi, and Javed Arif. Size of radial and ulnar artery in local population. 60:817–9, 10 2010.

[5] Azran Azhim. Measurement of blood flow velocity waveforms in the carotid, brachial and femoral arteries during head-up tilt. 2:1–6, 01 2008.

[6] Jose Carlos Baptista Silva, Andr Loureno Dias, Serafim Vincenzo Cricenti, and Emil Burihan. Anatomy of the basilic vein in the arm and its importance for surgery. 20:171, 07 2003.

[7] Jacopo Biasetti, Fazle Hussain, and T. Christian Gasser. Blood flow and coherent vortices in the normal and aneurysmatic aortas: a fluid dynamical approach to intraluminal thrombus formation. *Journal of The Royal Society Interface*, 8(63):1449–1461, 2011.

[8] Mary Beth Browning, Viviana Guiza, Brooke Russell, Jose Rivera, Stacy Cereceres, Magnus Höök, Mariah S Hahn, and Elizabeth M Cosgriff-Hernandez. Endothelial cell response to chemical, biological, and physical cues in bioactive hydrogels. *Tissue Engineering Part A*, 20(23-24):3130–3141, 2014.

[9] Yinghui Chen, Lei Zhang, David Zhang, and Dongyu Zhang. Wrist pulse signal diagnosis using modified gaussian models and fuzzy c-means classification. 31:1283–9, 09 2009.

[10] Bell DD and Rosental JJ. Arteriovenous graft life in chronic hemodialysis: A need for prolongation. *Archives of Surgery*, 123(9):1169–1172, 1988.

[11] Simon Gelman M.D. Ph.D. Venous function and central venous pressurea physiologic story. *Anesthesiology*, 108(4):735–748, 2008.

[12] William H. Bay, Mitchell L. Henry, J Michael Lazarus, Nancy L. Lew, Jie Ling, and Edmund G. Lowrie. Predicting hemodialysis access failure with color flow doppler ultrasound. 18:296–304, 07 1998.

[13] James J. Hathcock. Flow effects on coagulation and thrombosis. *Arteriosclerosis, Thrombosis, and Vascular Biology*, 26(8):1729–1737, 2006.

[14] Alun D. Hughes, Justin E. Davies, Darrel Francis, Jamil Mayet, and Kim H. Parker. Peripheral augmentation index and wave reflection in the radial artery. *Hypertension*, 51(6):e45–e46, 2008.

[15] .K Shoemaker M.J MacDonald R.L Hughson. Time course of brachial artery diameter responses to rhythmic handgrip exercise in humans. *Cardiovascular Research*, 35(1):125–131, 1997.

[16] Barbara M. Johnston, Peter R. Johnston, Stuart Corney, and David Kilpatrick. Non-newtonian blood flow in human right coronary arteries: steady state simulations. *Journal of Biomechanics*, 37(5):709 – 720, 2004.

[17] Susann J. Jrhult, Johan Sundstrm, and Lars Lind. Brachial artery hyperemic blood flow velocities are related to carotid atherosclerosis. *Clinical Physiology and Functional Imaging*, 29(5):360–365.

[18] R Y Kanterman, T M Vesely, T K Pilgram, B W Guy, D W Windus, and D Picus. Dialysis access grafts: anatomic location of venous stenosis and results of angioplasty. *Radiology*, 195(1):135–139, 1995. PMID: 7892454.

[19] Zaher Kharboutly, Valerie Deplano, Eric Bertrand, and Cecile Legallais. Numerical and experimental study of blood flow through a patient-specific arteriovenous fistula used for hemodialysis. 32:111–8, 12 2009.

[20] John Lane, Tazo Inui, Andrew Barleben, and Eugene Golts. Brachial artery flow assessment by duplex ultrasound predicts dialysis access steal syndrome. 43:50, 08 2017.

[21] Sang-Wook Lee, David S. Smith, Francis Loth, Paul F. Fischer, and Hisham S. Bassiouny. Numerical and experimental simulation of transitional flow in a blood vessel junction. 51:1–22, 11 2007.

[22] Catherine Loudon and Antoinette Tordesillas. The use of the dimensionless womersley number to characterize the unsteady nature of internal flow. *Journal of Theoretical Biology*, 191(1):63 – 78, 1998.

[23] Jennifer M. MacRae, Christine Dipchand, Matthew Oliver, Louise Moist, Charmaine Lok, Edward Clark, Swapnil Hiremath, Joanne Kappel, Mercedeh Kiaii, Rick Luscombe, Lisa M. Miller, and on behalf of the Canadian Society of Nephrology Vascular Access

Work Group. Arteriovenous access failure, stenosis, and thrombosis. *Canadian Journal of Kidney Health and Disease*, 3:2054358116669126, 2016.

[24] Jan Malk, Vladimir Tuka, Z Kasalova, Eva Chytilova, M Slavikova, P Clagett, I Davidson, B Dolmatch, D Nichols, and Maurizio Gallieni. Understanding the dialysis access steal syndrome. a review of the etiologies, diagnosis, prevention and treatment strategies. 9:155–66, 07 2008.

[25] Halsz G Matolcsi K., Brdossy G. Simulation of saline solution injection into a venous junction. In *IFMBE Proceedings*, volume 37, pages 343–346. Springer, Berlin, Heidelberg, 2011.

[26] Gregg A. Miller, Naveen Goel, Alexander Friedman, Aleksandr Khariton, Manish C. Jotwani, Yevgeny Savransky, Konstantin Khariton, William P. Arnold, and Dean C. Preddie. The miller banding procedure is an effective method for treating dialysis-associated steal syndrome. *Kidney International*, 77(4):359 – 366, 2010.

[27] Anna Ooue, Tomoko K. Ichinose, Yoshimitsu Inoue, Takeshi Nishiyasu, Shunsaku Koga, and Narihiko Kondo. Changes in blood flow in conduit artery and veins of the upper arm during leg exercise in humans. *European Journal of Applied Physiology*, 103(3):367–373, Jun 2008.

[28] Christopher P. Johnson, Yong-ran Zhu, Carrie Matt, Corey Pelz, Allan M. Roza, and Mark B. Adams. Prognostic value of intraoperative blood flow measurements in vascular access surgery. 124:729–37; discussion 737, 11 1998.

[29] M. Rocco, J.T. Daugirdas, T.A. Depner, J. Inrig, R. Mehrotra, M.V. Rocco, R.S. Suri, D.E. Weiner, N. Greer, A. Ishani, R. MacDonald, C. Olson, I. Rutks, Y. Slinin, T.J. Wilt, H. Kramer, M.J. Choi, M. Samaniego-Picota, P.J. Scheel, K. Willis, J. Joseph, and L. Brereton. Kdoqi clinical practice guideline for hemodialysis adequacy: 2015 update. *American Journal of Kidney Diseases*, 66(5):884–930, 2015. cited By 115.

[30] Kittipan Rerkasem Sasikarn Khruasingkeaw, Yottana Khunatorn and Tanop Srisuwan. Wall shear stress distribution in arteriovenous graft anastomosis using computational fluid dynamics. *International Journal of Pharma Medicine and Biological Sciences*, 5(4):385–403, 2016.

[31] MASSIMO STEFANO SILVETTI, SILVIA PLACIDI, ROSALINDA PALMIERI, DANIELA RIGHI, LUCILLA RAV, and FABRIZIO DRAGO. Percutaneous axillary vein approach in pediatric pacing: Comparison with subclavian vein approach. *Pacing and Clinical Electrophysiology*, 36(12):1550–1557.

[32] Vladimir Subbotin. Analysis of arterial intimal hyperplasia: Review and hypothesis. 4:41, 02 2007.

[33] Sonia Tabakova, Nikolay Kutev, and Stefan Radev. Application of the carreau viscosity model to the oscillatory flow in blood vessels. *AIP Conference Proceedings*, 1690(1):040019, 2015.

[34] Vincent T. Turitto and Hans R. Baumgartner. Platelet interaction with subendothelium in flowing rabbit blood: Effect of blood shear rate. *Microvascular Research*, 17(1):38 – 54, 1979.

[35] K. Van Canneyt, U. Morbiducci, S. Eloot, G. De Santis, P. Segers, and P. Verdonck. A computational exploration of helical arterio-venous graft designs. *Journal of Biomechanics*, 46(2):345–353, 2018.

[36] Vignon-Clementel, Figueroa, Jansen, and Taylor. Outflow boundary conditions for 3d simulations of non-periodic blood flow and pressure fields in deformable arteries. *Computer Methods in Biomechanics and Biomedical Engineering*, 13(5):625–640, 1 2010.

[37] Frank M. White. *Viscous Fluid Flow*. McGraw Hill, New York New York, 2006.

[38] Alireza Yazdani, He Li, Jay D. Humphrey, and George Em Karniadakis. A general shear-dependent model for thrombus formation. *PLOS Computational Biology*, 13(1):1–24, 01 2017.

[39] Jonathan M. Zalger. A fluid-structure interaction analysis of the human aortic arch under inertial load. Master's thesis, Ryerson University, 2008.

CFD Analysis of AVG Configurations, Williams, M.S. 2018